Atmospheric Environment 189 (2018) 227–234

Contents lists available at ScienceDirect

Atmospheric Environment

journal homepage: www.elsevier.com/locate/atmosenv

Variations of Siberian High Position under climate change: Impacts on winter pollution over north China

Beixi Jia[a], Yuxuan Wang[a,b,*], Shan Huang[a], Yang Nan[a], Xuwen Zhou[c]

[a] Department of Earth System Science, Tsinghua University, Beijing, China
[b] Department of Earth and Atmospheric Sciences, University of Houston, Houston, TX, United States
[c] Hebei Climate Center, Shijiazhuang, Hebei, China

ARTICLE INFO

Keywords:
Synoptic-scale circulation
Siberian High Position index
North China
Winter AOD
Future air quality

ABSTRACT

We examined the correlations between winter aerosol optical depth (AOD) in North China (NC) and three synoptic-scale meteorological indices from 2001 to 2016, including the Siberian High intensity (SHI), East Asian Winter Monsoon intensity (EAWMI), and the Siberian High Position index (SHPI). To separate the influences from meteorology and emissions, NC AOD was detrended by subtracting a linear increasing trend from 2001 to 2013 and a decreasing trend from 2014 to 2016, in correspondence with reported changes in Chinese anthropogenic emissions during the same period. The SHPI explains 37% of the variability in the detrended NC AOD and 83% of the high SHPI winters correspond to high AOD. By contrast, the SHI and EAWMI show little correlation with the observed AOD variability. To project the SHPI in the future climate, we used the ensemble of six global circulation models (GCMs) which were found capable of reproducing the climatic spatial distribution and the longitudinal variability of the Siberian High from 1956 to 2005. The ensemble results show that the frequency of high SHPI winters and consequently more polluted conditions would increase by 29%, 61%, and 100% under RCP2.6, RCP4.5 and RCP8.5 until 2099. There are 11 out of the 25 GCMs examined here that project the possibility of high SHPI conditions to increase under RCP8.5. This indicates changes in the Siberian High position induced by increasing global greenhouse gas (GHG) emissions can lead to more winter pollution in North China in the future.

1. Introduction

High levels of fine particulate matter with aerosol dynamic diameters equal to or less than 2.5 μm ($PM_{2.5}$) are not only associated with increased morbidity and mortality but also affect climate and economic activities (Lelieveld et al., 2015; Chen and Wang, 2015). Extreme haze events in winter have been on the rise during the past decade over the populous North China (NC) region, which can be attributed to the combined effects of increasing anthropogenic emissions and unfavorable weather conditions (Niu et al., 2010; Guo et al., 2011; Gao et al., 2016). Some severe haze events saw levels of $PM_{2.5}$ in many cities exceeded 500 $\mu g/m^3$, such as those occurred in January 2013, December 2015 and 2016 (Wang et al., 2014c; Wang et al., 2014a; Xue et al., 2016; Yin and Wang, 2017).

While pollutant emissions from human activities are the underlying cause for high $PM_{2.5}$ levels over NC, meteorological factors also play an important role (Huang et al., 2014; Zhang et al., 2014; Wang et al., 2014b). Many indices characterizing synoptic- or local-scale meteorological patterns have been proposed to explain the variability of winter air quality in NC. On the large scale, the East Asian winter monsoon (EAWM) is the most important circulation pattern over East Asia in winter, influencing the weather and climate in East Asia and even the whole Northern Hemisphere (Gong and Ho, 2002; Chernokulsky et al., 2013; Wang and Chen, 2014). The EAWM is characterized by the northwesterly winds along the coast of East Asia, which is caused by the pressure gradient between the Siberian High (SH) and the Aleutian Low (Chang and Lu, 2012). Wang et al. (2014b) calculated daily SH intensity index (SHI) in January 2013 and found during the haze period, the intensity of the SH is much lower than its climatic average from 1981 to 2010. Gao and Xiang (2015) analyzed winter haze days and the synoptic-scale circulation during 1981–2010 and found circulation patterns with a stronger SH and a stronger Aleutian Low were associated with fewer haze events. Our recent study (Jia et al., 2015) analyzed the anomalous circulation pattern during the severe haze month of January 2013 and established a Siberian High position index (SHPI) which shows good correlations with satellite-

* Corresponding author. Department of Earth System Science, Tsinghua University, Beijing, China.
E-mail address: ywang246@central.uh.edu (Y. Wang).

https://doi.org/10.1016/j.atmosenv.2018.06.045
Received 25 January 2018; Received in revised form 19 June 2018; Accepted 28 June 2018
Available online 05 July 2018
1352-2310/

retrieved aerosol optical depth (AOD) - a good indicator of surface $PM_{2.5}$ - over NC from 2001 to 2013. The SHPI depicts the mean longitudinal position of the SH. High values of SHPI (e.g. the winter of 2003 and January 2013) were found to be associated with extremely high values of winter-mean and monthly-mean AOD over NC due to conditions of low wind speed and high relative humidity over NC. On the local scale, Cai et al. (2017) developed a haze weather index (HWI) using vertical temperature gradient, meridional wind speed on 850 hPa, and zonal wind speed on 500 hPa. They found 70% of the HWI > 1 days in winters from 2009 to 2015 were severe haze days in Beijing. Zou et al. (2017) defined a pollution potential index characterizing both horizontal and vertical ventilation capability, which correlates well with surface PM_{10} (fine particulate matter with aerosol dynamic diameters equal to or less than 10 μm) (r = 0.92) and $PM_{2.5}$ (r = 0.79) in Beijing on the interannual time scale from 1981 to 2015.

Many of the aforementioned indices including the SHPI were developed based on air quality and meteorological data during the period from as early as the 1960s to the early 2010s, during that time emissions of air pollutants in China have increased rapidly. In order to separate the effect of emissions from that of meteorology, our prior study (Jia et al., 2015) assumed that air pollution time series would feature a monotonically increasing trend as a result of increasing emissions. The departure from that trend would then be caused by meteorology-related variability. In that study, a linear trend was subtracted from the time series of AOD between 2001 and 2013 to minimize the influence of increasing emissions on the AOD variability.

However, Chinese anthropogenic emissions have started to decrease recently. The year at which the amount of emissions started to decrease may be different for different pollutants. For example, SO_2 levels were observed to decrease around 2007 due to the implementation of SO_2 emission reduction measures during the 11th Five-Year Plan (2006–2010) (Nickolay et al., 2016), whereas NOx emissions kept increasing during the same period (Wang et al., 2014b). The most recent landmark event is the publication and implementation of the Air Pollution Prevention and Control Action Plan in 2013. Ample evidence has been drawn from *in situ* and satellite data that showed noticeable decreases in SO_2 and NO_2 concentrations together with $PM_{2.5}$ levels after 2013 (Nickolay et al., 2016; Ronald, 2017; Li et al., 2017). Annual mean concentrations of SO_2, NO_2, and $PM_{2.5}$ over China in 2016 were found to be 35%, 12%, and 26% lower from their respective levels in 2014 (Li et al., 2017). Therefore, 2013 may be taken as the emission turning point for many air pollutants in China. As the aforementioned meteorological indices for air pollution were developed under the setting of increasing emissions, it is not clear whether they would still apply after 2013. Therefore, a purpose of this study is to answer this question by examining the record of some synoptic-scale meteorological indices developed previously over a longer time period, covering the most recent years after 2013. The meteorological indices to be examined here are all pertaining to synoptic-scale circulations, including SHI, SHPI, and the East Asian Monsoon intensity index (EAWMI).

These meteorological indices are particularly useful to project future air quality changes associated with different climate scenarios. A typical practice is to apply the observed relationships of air quality and meteorological indices to future projections of those indices from the ensemble of climate models. Cai et al. (2017) projected the future variation of HWI under Representative Concentration Pathway 8.5 (RCP8.5) and found the frequency of HWI will increase during 2050–2099 compared to 1950–1999, indicating the haze frequency in Beijing will become more severe under global warming. Tai et al. (2012) found the variations of annual mean $PM_{2.5}$ in the US is strongly correlated with synoptic periods on the interannual scale. Applying this relationship to the Global circulation model (GCM) ensemble mean results, they projected a weak increase of annual mean $PM_{2.5}$ over the eastern US and a weak decrease over the Pacific Northwest in the 2050s under the A1B scenario (rapid economic growth with a balance across all sources). Shen et al. (2017) quantified the influence of 2000–2050 climate change on $PM_{2.5}$ air quality across the contiguous US. They projected an increase of 0.4–1.4 $\mu g/m^3$ in annual mean $PM_{2.5}$ in the eastern US and a decrease of 0.3–1.2 $\mu g/m^3$ in the western US by the 2050s. Long-term observational $PM_{2.5}$ data are not available over NC due to the lack of *in situ* surface measurements. Previous studies have shown high temporal and spatial correlations between AOD and *in situ* $PM_{2.5}$ and as such, satellite-derived AOD has been widely used as a good indicator of surface $PM_{2.5}$ (Wang and Christopher, 2003; Ma et al., 2014; Xie et al., 2015; Li et al., 2015). Xie et al. (2015) found moderately high correlations (0.6) between daily AOD from the Moderate Resolution Imaging Spectroradiometer (MODIS) sensor and $PM_{2.5}$ at surface monitors in Beijing. Over the North China Plain region, the correlation between MODIS AOD and ground-based $PM_{2.5}$ in winter was reported as 0.59 (Guo et al., 2017). Thus, we used AOD retrieved from MODIS as the proxy data to represent the interannual variations of $PM_{2.5}$. Winters with high AOD (detrended AOD > 0) were defined as polluted winters. This study also projects future changes in NC AOD caused by projected future changes in the synoptic-scale indices following three RCPs (RCP2.6, RCP4.5, and RCP8.5).

The paper is organized as follows. Section 2 describes the data and methods used in the analysis. In section 3, we examine whether SHPI, SHI and EAWMI correlate with winter air quality over NC during the period of 2001–2016 covering both increasing and decreasing emissions. Section 4 evaluates GCMs in simulating the SH and from the evaluation, six GCMs are selected to project the future change of SHPI under RCP2.6, RCP4.5, and RCP8.5. We also examine the variations of SHPI in the historical runs forced by different forcings to discuss the potential reasons for high SHPI conditions.

2. Data

2.1. Aerosol optical depth and in situ $PM_{2.5}$

We used level-3 monthly gridded AOD at 550 nm retrieved from the Moderate Resolution Imaging Spectroradiometer (MODIS) sensor aboard both NASA EOS-Terra and Aqua satellite as the proxy data to represent the long-term variations of surface $PM_{2.5}$. The data are from December 2000 to February 2016 with a 1° × 1° resolution. The AOD values over bright surfaces were replaced by the Deep Blue aerosol retrieval (550 nm) at the same grid. MODIS AOD were obtained from NASA website (ftp://ladsweb.nascom.nasa.gov/allData/51).

To verify the variations of AOD in the recent years from 2014 to 2016, during which time AOD over NC shows a large decrease, we also analyzed *in situ* $PM_{2.5}$ over NC. The observational hourly $PM_{2.5}$ data are available at http://www.pm25.in/since November 2013. Similar to our previous study, the NC region is delineated by longitude from 115° E to 123° E, and by latitude from 30° N to 42° N. In situ $PM_{2.5}$ observations from 46 cities in NC were used for the verification of NC AOD. The average $PM_{2.5}$ for a city may contain several monitoring sites. For example, the average of 12 monitoring sites in Beijing is taken as the average $PM_{2.5}$ in Beijing.

2.2. Meteorological data and CMIP5 model results

We obtained meteorological parameters from National Centers for Environmental Prediction (NCEP) reanalysis (Kalnay et al., 1996) to calculate the meteorological indices and test their correlations with winter air quality in recent years. The variables include sea level pressure (SLP) and 850 hPa wind field with a resolution of 2.5° × 2.5°. The NCEP reanalysis data provide a historical record of more than 50 years from 1948 (Kistler et al., 2001), and were obtained from NOAA website (http://www.esrl.noaa.qov/psd/data/gridded/).

We also selected SLP projected by 25 GCMs that participated in the Coupled Model Intercomparison Project Phase 5 (CMIP5) and provided outputs from all three RCPs. Table 1 describes the general information

Table 1
The description of the 25 CMIP5 models used in this study.

Model	Center (country)	Resolution
BCC-CSM1.1	BCC (China)	128 × 64
BCC-CSM1-1-M	BCC (China)	320 × 160
BNU-ESM	GCESS, BNU (China)	128 × 64
CanESM2	CCCma (Canada)	128 × 64
CNRM-CM5	CNRM-CERFACS (France)	256 × 128
CSIRO-Mk3.6.0	CSIRO-QCCCE (Australia)	192 × 96
FIO-ESM	FIO (China)	128 × 64
IPSL-CM5A-LR	IPSL (France)	96 × 96
IPSL-CM5A-MR	IPSL (France)	144 × 143
MIROC5	MIROC (Japan)	256 × 128
MIROC-ESM	MIROC (Japan)	128 × 64
MIROC-ESM-CHEM	MIROC (Japan)	128 × 64
HadGEM2-ES	MOHC (UK)	192 × 145
MPI-ESM-LR	MPI-M (Germany)	192 × 96
MPI-ESM-MR	MPI-M (Germany)	192 × 96
MRI-CGCM3	MRI (Japan)	320 × 160
GISS-E2-H	NASA GISS (US)	144 × 90
GISS-E2-R	NASA GISS (US)	144 × 90
CCSM4	NCAR (US)	288 × 192
NorESM1-M	NCC (Norway)	144 × 96
NorESM1-ME	NCC (Norway)	144 × 96
HadGEM2-AO	NIMR-KMA (Korea)	192 × 145
GFDL-CM3	NOAA-GFDL (US)	144 × 90
GFDL-ESM2G	NOAA-GFDL (US)	144 × 90
CESM1-CAM5	NSF-DOE-NCAR (US)	288 × 192

of the models used in this study. The data include model results from historical runs and the RCP runs. The period of 1850–2005 is designated as the "historical period" in the modeling experiments of CMIP5. We chose the SLP from the GCM's 50-year (1956–2005) historical experiments for comparison with the SLP from the NCEP reanalysis. The results of historical runs using different forcings were also obtained to examine the reasons for high SHPI conditions. In CMIP5, a set of RCP scenarios is provided to explore the variations of climate under different climate policies (Moss et al., 2010; Taylor et al., 2012). Therein, RCP2.6 is a mitigation scenario, in which CO_2 emissions decrease from 2020, radiative forcing reaches 2.6 W/m^2 by 2100 and stabilizes after that (Taylor et al., 2012). RCP4.5 and RCP8.5 are the medium-low and high greenhouse gas emissions pathways leading to radiative forcings of 4.5 and 8.5 W/m^2 respectively at the end of the century (Moss et al., 2010). CO_2 emissions in RCP4.5 increase from 2000 to 2040 and decrease after that, and CO_2 emission in RCP8.5 keep increasing in the 21st century. SLP projected by the GCMs following the three RCPs from 2007 to 2099 were also obtained for the prediction of future frequency of extremely polluted winter. The GCM results were taken from http://cmip-pcmdi.llnl.gov/cmip5/.

3. Method

As discussed above, most synoptic-scale indices derived to date including the SHPI were developed under the background when both anthropogenic emissions and the frequency of haze events were increasing in China. Since the publication of the Air Pollution Prevention and Control Action Plan in 2013 and the stricter emission reductions since then, concentrations of SO_2, NO_2 and $PM_{2.5}$ have been decreasing after 2013. Fig. 1 compares the distribution of MODIS AOD between the 2011–2013 and 2014–2016 winter mean. Winter-mean AOD shows a significant decrease over the whole eastern China, and the largest decrease is seen over NC (black box in Fig. 1), where AOD decreased from 0.7 (2011–2013 winter mean) to 0.58 (2014–2016 winter mean). This decrease of AOD most likely reflects the decrease of emissions after 2013. In this analysis, we examine the ability of the synoptic-scale circulation indices to explain the winter AOD variability after 2013 when emissions started to decrease. Such assessment is the necessary step before one can use the future changes of those indices projected by the GCMs to project future air quality over NC. The indices include SHPI, SHI and EAWMI, and the definitions of the indices are adopted from the previous studies (Jia et al., 2015; Jeong et al., 2011; Hasanean et al., 2013; Wang and Jiang, 2004).

3.1. Validation of SHPI from 2001 to 2016

The winter mean NC AOD from 2001 to 2016 is shown in Fig. 2a. AOD shows a significant increasing trend from about 0.5 in 2001 to about 0.8 in 2013, followed by a sharp decrease to 0.5 in 2016. A linear regression gives a decreasing trend of 9.8% per year during 2013–2016. Consistent with the satellite data, a decreasing trend is also found in surface measurements of $PM_{2.5}$ over NC during the winters of 2014–2016 when those data were available. The NC-mean surface $PM_{2.5}$ decreased from about 118.7 μg/m^3 in winter 2014 to 86.2 μg/m^3 in winter 2016, corresponding to a decreasing trend is 16.3 μg/m^3 per year.

In our previous study (Jia et al., 2015), we defined the SHPI as the weighted mean longitude of all the grids within the 1023 hPa isobar over the broad region of 60–145°E and 30–65°N. A high SHPI indicates an eastward extension of the SH, which brings about conditions of lower wind speed and higher relative humidity over NC, both conducive for higher PM levels. Long-term mean winter SHPI from 2001 to 2016 is 99.1 and the standard deviation of SHPI from 2001 to 2016 is 1.7 (Fig. 2a). If we define high SHPI years as those with SHPI exceeding the mean value of SHPI plus half of its standard deviation (SHPI = 100.0), six years including 2001, 2003, 2007, 2013, 2014 and 2015 are high SHPI years. For example, SHPI in 2013 was 100.6, and SHPI in 2014 and 2015 were even higher than 100.6, indicating favorable synoptic-scale conditions for high AOD in winter. Therefore, the large decreasing trend in AOD after 2013 (Fig. 2a) should not be caused by meteorology. It is most likely due to decreasing emissions. Indeed, the concentrations of SO_2, NO_2, $PM_{2.5}$, and AOD have shown decreases after 2013, indicating the emission trend in NC during 2013–2016 would be different from that in 2001–2013.

The overall correlation efficient between SHPI and NC AOD from 2001 to 2016 is only 0.35. This low correlation is another indication that the emission turning point in 2013 needs to be considered. To do this, we estimated the trend in NC AOD using a piecewise linear equation. The year 2013 is set to be the turning point, and AOD from 2001 to 2013 and from 2014 to 2016 were detrended separately. The resulting linear regression of NC AOD from 2001 to 2013 (i.e., $AOD_{2001\text{-}2013} = 0.015 \times (\text{year-}2000) + 0.491$) gave an increasing trend of 1.5% year^{-1}, consistent with our previous study (Jia et al., 2015) ($r = 0.65$, $p < 0.05$). The decreasing trend in NC AOD from 2014 to 2016 is estimated to be 9.1% year^{-1} (i.e. $AOD_{2014\text{-}2016} = -0.091 \times (\text{year-}2000) + 0.762$). Since the length of the data record is limited after 2013, this decreasing trend is not statistically significant ($p = 0.35$), despite r being 0.66. Fig. 2a depicts the trend line from the piecewise regression (dashed red line) along with the raw time series of AOD (solid red line). While we still followed the conventional approach that the trend in AOD represents the influence of anthropogenic emissions, this trend was not taken as a monotonic function of time but reflects the emission turning point in 2013.

The interannual variations of AOD superimposed on this trend (i.e., de-trended AOD) were then taken to reflect the meteorological influences on AOD. Fig. 2b shows the variations of the detrended NC AOD and normalized SHPI, and the correlation between them is 0.61 ($p < 0.05$). The SHPI time series were normalized by their 2001–2016 mean and standard deviation. This suggests that the SHPI can explain more than 37% of interannual AOD variability when anthropogenic emissions had both increased and decreased in China, as long as the trend in emissions is properly considered. Among the six high SHPI years, five of them (83%) had high AOD (detrended AOD > 0); those years are 2001, 2003, 2007, 2013, and 2014. This suggests that the SHPI is better suited to explain the occurrence of severe winter

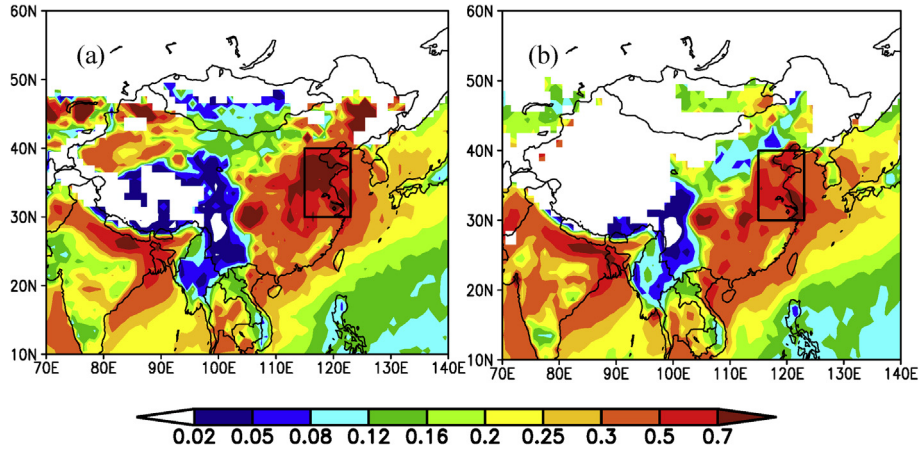

Fig. 1. Spatial distribution of winter mean MODIS AOD for (a) 2011–2013 mean and (b) 2014–2016 mean.

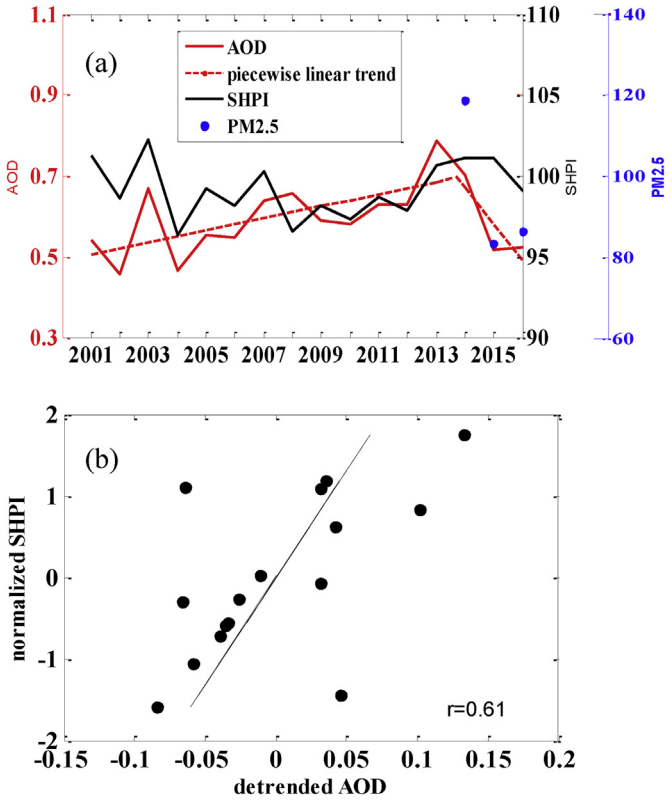

Fig. 2. (a) Interannual variations of winter mean NC AOD, SHPI, NC $PM_{2.5}$ (μg/m^3) and piecewise linear trend in NC AOD; (b) detrended NC AOD and normalized SHPI.

pollution in NC than the year-to-year variability.

3.2. Other synoptic-scale indices

The SH and EAWM are important circulation patterns affecting climate and air quality over East Asia in winter (Niu et al., 2010; Xu et al., 2016; Cheng et al., 2016). Niu et al. (2010) identified the increasing frequency of fog over East China in winter from 1976 to 2007 was linked with the decreasing regional mean wind speed over East China which in turn was due to the decreasing intensity of EAWM. Xu et al. (2016) found a negative correlation between EAWM wind and the number of haze days over central East China region from 1961 to 2011. The interannual variability in the intensity of the SH as described above may be connected with changes in other aspects of the SH (e.g. its intensity) and with the EAWM. Thus, in this section we analyze the variations of SH intensity and EAWM intensity during the same period. SHI is defined as the mean SLP over northern Mongolia between 80 and 120°E and 40–65°N (Jeong et al., 2011; Hasanean et al., 2013). EAWMI is defined as the mean wind speed on 850 hPa over the region between 115 and 145°E and 25–50°N, following Wang and Jiang (2004). High EAWMI and SHI are thought to bring stronger northwesterly winds in the lower troposphere, thus favorable for the dispersion of pollution in NC.

Figure S1 shows the time series of SHI and EAWMI from 2001 to 2016. Comparing to 2001–2012, SHI and EAWMI do not have any significant changes from 2013 to 2016, indicating the decreasing trend in NC AOD is not driven by the intensification of the SH or EAWM. The variations of normalized SHI, EAWMI, and piecewisely detrended NC AOD is shown in Fig. 3. The correlation of SHI and EAWMI with detrended NC AOD is −0.11 (p = 0.69) and −0.40 (p = 0.12), respectively, much lower than that between SHPI and detrended NC AOD. Similar to the approach to select high SHPI years, we define low SHI (EAWMI) year as the mean value during 2001–2016 minus half the standard deviation. Eight (four) years during 2001–2016 were low SHI (EAWMI) years, and only two (one) of them were associated with high AOD. Thus, compared with SHI and EAWMI, the SHPI is a better index in capturing the variability in NC AOD and the occurrence of high AOD winters associated with synoptic-scale circulation. Therefore, the SHPI is the only index used in the following analysis of projecting the variations of wintertime NC AOD due to synoptic-scale meteorology in the future climate.

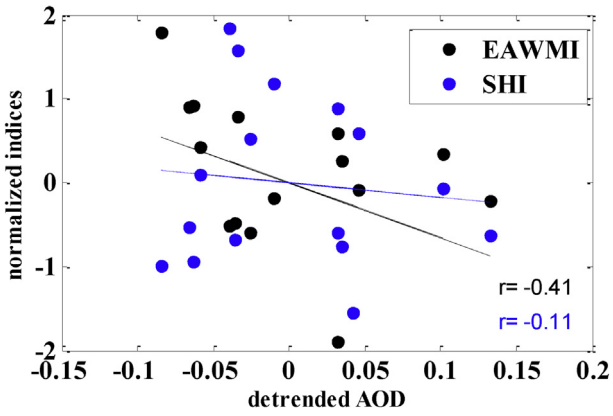

Fig. 3. Normalized EAWMI, SHI and detrended NC AOD.

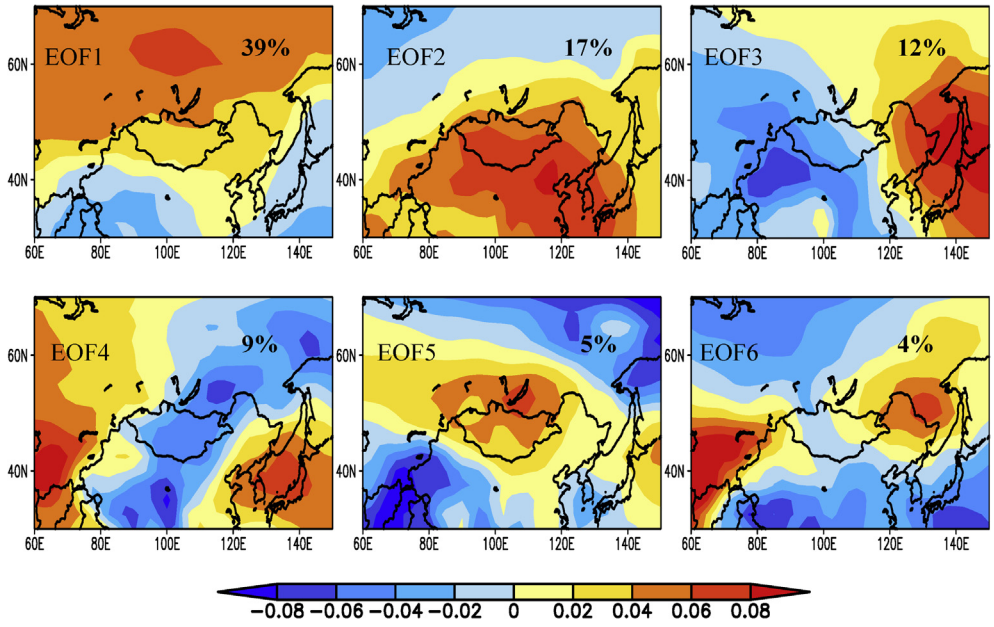

Fig. 4. First six EOF spatial patterns of standardized winter NCEP SLP from 1956 to 2005.

4. Results

4.1. Evaluation of GCMs and future projection of SHPI

GCMs are widely used in the prediction of synoptic-scale circulations and regional climate. Previous studies have shown that the CMIP5 models have skills in simulating synoptic-scale circulations and regional meteorology. For example, Brown et al. (2013) evaluated 35 CMIP5 models in simulating West Pacific Monsoon and found they were capable of reproducing the synoptic-scale seasonal cycle of low-level winds and rainfall associated with this monsoon. Yao et al. (2013) analyzed monthly mean extreme temperatures in Coupled Model Intercomparison Project Phase 3 (CMIP3) and CMIP5 models and found the CMIP5 models performed better in simulating temperature extremes and showed improvements on the local grid-cell scale than the CMIP3 models. In this section, we first examine the performance of the CMIP5 GCMs in simulating the SH, from which four GCMs with good predictive capability are selected. We then derive future changes in SHPI from those GCMs under different warming scenarios and project the future change of NC AOD based on the SHPI changes.

Table 1 describes the general information of the 25 GCMs used in this study. Since the GCMs have different resolutions, we used bilinear interpolation to interpolate the GCM results onto 2.5°x2.5°grid for an easier comparison with the NCEP reanalysis. Figure S2 shows the long-term (1956–2005) mean distribution of winter SLP over the Siberian region from the NCEP reanalysis and as simulated by the 25 GCMs. The predominant feature of NCEP winter SLP is a high pressure system over the Siberian region centered in Mongolia and a low pressure system over the North Pacific centered in the Aleutian region, corresponding to the SH and the Aleutian Low respectively. Most GCMs capture this feature and the spatial distribution of climatic winter SLP over East Asia, except for the HadCM3 and CSIRO model in which the location of the high pressure center is placed northward, nearly reaching the Arctic. To quantify the GCM performance, the spatial correlation coefficient between simulated winter SLP over the Siberian region (black box in Figure S2) from each of the GCMs and the NCEP reanalysis is calculated. If the correlation of 0.6 is chosen as a criterion, 21 out of the 25 GCMs capture the long-term mean spatial distribution of winter SLP over the Siberian region.

The high spatial correlation coefficients indicate most GCMs can capture the spatial distribution of winter SLP. We then evaluated the interannual variations of the SH in the GCMs, in which two SH indices were tested: the conventionally used SHI and the SHPI we developed. Correlation coefficients of the two indices between NCEP and GCMs are also calculated. Only two GCMs (GISS-H and CMCC-CESM) have a significant positive correlation ($p < 0.1$) with the SHPI from the NCEP. Although 15 GCMs have positive correlations with the SHI from the NCEP, none of them is significant. This indicates that most GCMs are not suitable to predict year-to-year changes of the intensity and the position of the SH. This may be because the free-running GCMs do not assimilate observations during the simulation. Therefore, we seek other ways to evaluate the ability of GCMs simulating the variability of the SH.

Empirical Orthogonal Functions (EOFs) are often used in the analysis of the variability of atmospheric variables (Fiore et al., 2003; Weaver and Nigam 2008; Shen et al., 2015). We applied EOF to decompose the interannual variability of winter mean SLP in NCEP over 1956 to 2005. From the first six EOF patterns from NCEP, we chose one SHPI-related pattern which displays the longitudinal variations of the SH, and took the variance contribution of this pattern as the contribution of the SHPI to the interannual variability of SLP over the Siberian region. This variance contribution was then used as the criterion to evaluate the ability of the GCMs in simulating the variability of the SHPI, if the same EOF analysis applied to the GCM SLPs can reveal the SHPI-related pattern.

The first six EOF loadings of standardized winter mean NCEP SLP from 1956 to 2005 are shown in Fig. 4. Altogether, the six EOFs explain 86% of the variance in winter SLP over northern Asia, and the first EOF pattern (EOF1) explains 39% of the variance. EOF1 displays opposite loadings over the East Asian continent and over the Pacific, indicating the opposite variations of SLP over the continent and over the sea. The time series of EOF1 (EOF-T1) were found to have a high correlation of 0.86 with the SHI, indicating the years with high EOF1 loadings were most likely associated with strong SH intensity. Therefore, EOF1 can be linked with the variability in the intensity of the SH.

The second EOF pattern (EOF2) explains 17% of the variance in SLP. It depicts the opposite variations of SLP between the south and north of the Siberian region, which may indicate the meridional variations of the SH. The third EOF pattern (EOF3) depicts the longitudinal variations of the SH because there are positive and negative EOF loadings over east and west Mongolia respectively, which is most similar to the SHPI pattern spatially. The EOF3 explains 12% of the variance in SLP. The

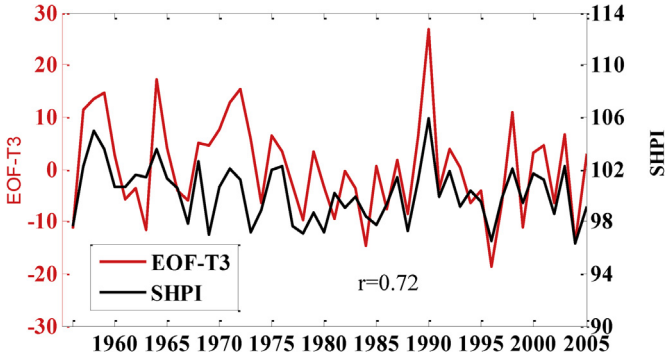

Fig. 5. Time series of EOF-T3 and SHPI from 1956 to 2005.

time series of EOF3 (EOF-T3) were found to have a good correlation of 0.72 with the NCEP SHPI (Fig. 5), indicating the years with high EOF3 loadings were likely high SHPI years. For example, high EOF3 loadings were seen in 1990 and 2003, and the SHPI in these years were also high. Given the good spatial and temporal association between the EOF3 and SHPI, this pattern is selected as the SHPI-related pattern in the following analysis. Since the EOF1 represents the SHI and EOF3 represents the SHPI, which are two separate EOF patterns that represent the intensity and the longitudinal position of the SH respectively, this explains why the SHI and SHPI do not have high correlations between themselves on the interannual time scale (Jia et al., 2015). Among the remaining three EOF patterns, the sixth pattern (EOF6) appears to also resemble the SHPI pattern spatially. However, the correlation between its time series and the time series of SHPI is much weaker (r = 0.04). Thus, among the six patterns, EOF3 best captures the spatial and temporal distribution of SLP over northern Asia in high and low SHPI years.

The next step is to analyze the EOF patterns of the SLP from the 25 GCMs from 1956 to 2005, select one EOF pattern from each GCM that depicts the longitudinal variations of the SH, and evaluate the variance contributions of the GCM-derived pattern against that from the NCEP as the criteria to select the GCMs. The first EOF pattern from each of the GCMs is shown in Figure S3, and the spatial correlation coefficients between the NCEP EOF1 and the GCM EOF1 (Table S2) were found to be higher than 0.7 for all the GCMs. This indicates the GCMs are good at reproducing the spatial contrast between SLP over land and the ocean (i.e., the opposite variations of SLP over East Asia and over the Pacific as seen in the NCEP EOF1), which is to be expected. The variance contribution of the EOF1 in the 25 GCMs ranges from 55% to 72%, which is a lot higher than the variance contribution of 39% from the NCEP EOF1. This discrepancy partly explains why the majority of the GCMs do not capture the interannual variability of the SHI. To choose one EOF pattern that depicts the longitudinal variations of the SH, we calculated the spatial correlation between the NCEP EOF3 (i.e. the SHPI pattern) and five remaining EOF patterns in each of the GCMs, and chose one EOF pattern from each GCM that resembles the spatial distribution of the NCEP EOF3. Table 2 shows the correlation coefficient between the NCEP EOF3 and the chosen EOF pattern from each of the GCMs and the variance contribution (VC) of that pattern. The correlation coefficients shown in Table 2 are higher than 0.6 in 23 of the 25 GCMs, however the VC of the chosen GCM patterns ranges widely, from 3% to 13%. By comparison, the VC of the NCEP EOF3 is 12%, and the VC of the proceeding (EOF2) and following EOF (EOF4) is 17% and 9% respectively. Therefore, we chose the GCMs with the VC lying between 17% (VC of the NCEP EOF2) and 9% (VC of the NCEP EOF4) as the ones being able to reproduce the historical (1956–2005) variations of the longitudinal variability of the SH and thus the SHPI. There are eight GCMs that pass this VC test: BCC-ESM1-1-M, BNU-ESM, CNRM-CM5, CSIRO, IPSL-CM5-MR, MRI-CGCM3, CCSM4 and CESM1-CAM5. Since the IPSL-CM5-MR and CSIRO model has a low correlation (< 0.6) with the NCEP field in terms of the long-term mean SLP over the Siberian region, they are excluded from the list. Therefore, six GCMs (BCC-ESM1-1-M, BNU-ESM, CNRM-CM5, MRI-CGCM3, CCSM4 and CESM1-CAM5) out of the initial 25 CMIP5 models were selected for further analysis of their projected SHPI variability in the 2100s under different RCP scenarios. The chosen EOF patterns of six GCMs are shown in Figure S4.

Table 2
Spatial correlation coefficients between NCEP EOF3 and chosen GCM EOF pattern.

Model	R	VC
BCC-CSM1.1	0.75	5%
BCC-CSM1-1-M	0.58	11%
BNU-ESM	0.82	12%
CanESM2	0.74	5%
CNRM-CM5	0.76	9%
CSIRO	0.80	11%
FIO-ESM	0.67	6%
IPSL-CM5A-LR	0.81	5%
IPSL-CM5A-MR	0.70	9%
MIROC5	0.75	5%
MIROC-ESM	0.63	6%
MIROC-ESM-CHEM	0.63	3%
HadGEM2-ES	0.74	4%
MPI-ESM-LR	0.67	5%
MPI-ESM-MR	0.64	4%
MRI-CGCM3	0.63	14%
GISS-R	0.65	4%
GISS-H	0.55	8%
CCSM4	0.60	13%
NorESM1-M	0.64	4%
NorESM1-ME	0.61	3%
HadGEM2-AO	0.64	4%
GFDL-CM3	0.72	4%
GFDL-ESM2G	0.73	6%
CESM1-CAM5	0.77	10%

4.2. Frequency of high SHPI in future climate and possible reasons

To project future changes of the SHPI in different RCPs, we first compiled the ensemble mean SLP from the six GCMs selected from the previous step under different forcings. The multi-model mean SLP fields were used to calculate the SHPI in the historical run from 1956 to 2005 and under three RCPs from 2007 to 2099. The model-derived mean historical SHPI is 96.6. The mean projected SHPI from 2007 to 2099 under the three RCPs is 96.4 (RCP2.6), 96.4 (RCP4.6), and 96.8 (RCP8.5), with the standard deviation 1.0 (RCP2.6), 1.0 (RCP4.5) and 0.9 (RCP8.5). Only RCP8.5 has the projected mean SHPI higher than the historical mean. The difference is however only 0.2, compared to the standard deviation of 0.9 of the ensemble mean SHPI from 1956 to 2005, and thus the difference is not significant.

The mean SHPI represents the mean longitudinal position of the SH, which is not the best metric to be related with the frequency of extreme pollution. In the previous section, we find a better association between high SHPI years and high AOD years. Therefore, we use the model-simulated frequency changes of extreme SHPI values to project how the frequency of severely polluted winter would change in different RCPs. Fig. 6 shows the cumulative frequency distribution of historical SHPI and the SHPI under the three RCPs. To compare how the frequency of extremely high SHPI conditions would change in the future projections compared to the historical run, we chose a certain value of SHPI as a threshold of high SHPI conditions. From 1956 to 2005, the frequency that the SHPI is higher than 97.6 occurred about once every ten years, thus 97.6 was selected as the threshold to screen for high SHPI in the future projection. The occurrence of the SHPI exceeding this threshold during 2007–2099 is 12, 15, and 19 times under RCP2.6, RCP4.5 and RCP8.5, respectively, and the corresponding frequency is 1.3, 1.6 and 2.0 times every ten years. Comparing to the historical frequency of once

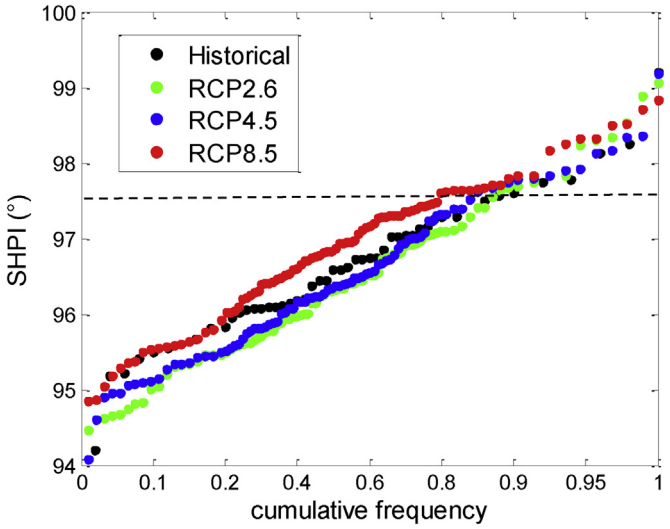

Fig. 6. Cumulative frequency of ensemble mean historical SHPI and SHPI from six selected GCMs under three RCPs. The dash line indicates SHPI = 97.56, the threshold.

per ten years, the occurrence of high SHPI conditions would increase in the future under three RCPs, and doubles under RCP8.5, indicating the frequency of severely polluted winter would increase significantly under RCP8.5.

Since the frequency of high SHPI conditions in the future varies by a factor of 1.5 under the low GHG emission pathways (RCP2.6) and the high GHG emission pathways (RCP8.5), we further examined the role that GHG emissions play in the occurrence of high SHPI conditions by comparing the results of the six GCMs from the historical experiments of GHG forcings only and natural forcings only. In the historical runs of natural forcings, only the solar radiation and volcanic aerosols change with time; in the historical runs forced by GHGs, only GHG emissions change with time. The multi-model mean value of SHPI is 96.1, 95.7 and 95.8 in the three historical experiments with all forcings, GHG only and natural forcings only, respectively, and the corresponding occurrence of SHPI exceeding the threshold of 97.6 during the historical simulation period is five, two, and five times (Fig. 7). This indicates high SHPI conditions are more related to the change of natural forcings including solar radiation and volcano aerosols comparing with the change of GHGs during 1956–2005. In the historical experiment forced only by

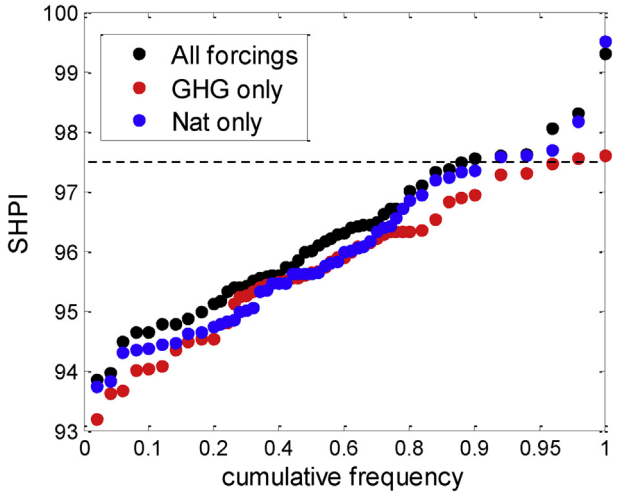

Fig. 7. Cumulative frequency of ensemble mean SHPI from six selected GCMs in historical run from 1956 to 2005 forced by all forcings (black), by GHG emissions only (red), and by natural forcings only (blue).

increasing GHG emissions during 1956–2005, exceedances of the SHPI threshold occur twice in 50 years, indicating increasing GHG emissions is also conducive for the occurrence of high SHPI conditions.

5. Conclusion

In this study, we investigated the relations between winter synoptic-scale circulations over East Asia including the SH and the EAWM with NC AOD during 2001 and 2016 when anthropogenic emissions kept changing. The anthropogenic emissions before 2010 in China kept increasing. After the publication of the Air Pollution Prevention and Control Action Plan in 2013, the concentrations of pollutants started to decrease. To separate the influences of meteorology and changing emissions, a piecewise linear regression is applied on NC AOD from 2001 to 2013 and from 2014 to 2016 separately. The piecewise linear regression of NC AOD gave an increasing trend of 1.5% year^{-1} from 2001 to 2013 and a decreasing trend of 9.8% year^{-1}from 2014 to 2016. The trends in NC AOD were taken to reflect the influence of emissions on NC AOD, and the interannual variations of AOD superimposed on this trend were then taken to reflect the meteorological influences on AOD.

The correlations between three synoptic-scale meteorological indices including the SHPI, EAWMI and the SHI with detrended NC AOD were examined from 2001 to 2016. The interannual variations of detrended NC AOD can be well explained by SHPI (r = 0.61) and 83% of the high SHPI years correspond to high AOD. However, the SHI and EAWMI show poor skill in reproducing NC AOD interannual variability, and no associations were found between low SHI (EAWMI) and high NC AOD. We show that the SHPI is the best synoptic-scale index among the three examined here in capturing the AOD variability in NC. Thus, the SHPI is the only index used in projecting the variations of wintertime NC AOD using GCM ensemble mean results.

We examined 25 CMIP5 GCMs in simulating the long-term mean spatial distribution of winter SLP over East Asia and the interannual variations of the SH from 1956 to 2005. Results show most GCMs capture the spatial distribution of NCEP winter SLP over the Siberian region while none of them are suitable to reproduce the interannual variations of the SHPI in NCEP. Since EOF is widely used to examine the interannual variability of the atmospheric variables, we adopted EOF to examine the SHPI-related SLP variability in GCMs. The variance contribution of the SHPI-related EOF pattern in GCMs is taken as the criteria to select GCMs that reproduce the longitudinal variability of the SH. Six GCMs including BCC-ESM1-1-M, BNU-ESM, CNRM-CM5, MRI-CGCM3, CCSM4 and CESM1-CAM5 were selected at last for further analysis of their projected SHPI variability in the 2100s under different RCP scenarios. The ensemble mean results of the six GCMs reveal the frequency of high SHPI threshold (97.6) would double in the future under RCP8.5, indicating severely polluted winter would occur more frequently in NC in the warming climate. Similar conclusions were made by Cai et al. (2017), and they concluded that the frequency and persistence of Beijing haze events would increase under RCP8.5.

To examine the role that GHG emissions and natural forcings play in the occurrence of high SHPI conditions, we analyzed the variations of SHPI from 1956 to 2005 in historical runs forced by different forcings. The high SHPI threshold occurs five times, twice and five times during 1956–2005 in historical run with all forcings, only GHG forcings and only natural forcings. Thus, we concluded that the extreme SHPI conditions are more related to the change of natural forcings, and the increasing GHG emissions from 1956 to 2005 are also favorable for high SHPI conditions.

The relationship between the SHPI and NC AOD under the changing emissions is examined during 2001–2016, a relatively short period. The decreasing trend in NC AOD from 2014 to 2016 is not significant due to the limited length of time series, although mean NC AOD shows a large decrease from about 0.7 in 2014 to 0.5 in 2016. The SHPI-NC AOD relationship under changing emissions, especially under the decreasing

emissions may require verification with longer-term observations.

Acknowledgement

This research was partly supported by the National Key Basic Research Program of China (2014CB441302). Yuxuan Wang acknowledges support from NSF AGS 1645062.

Appendix A. Supplementary data

Supplementary data related to this article can be found at https://doi.org/10.1016/j.atmosenv.2018.06.045.

References

Brown, J.R., Colman, R.A., Moise, A.F., Smith, I.N., 2013. The western Pacific monsoon in CMIP5 models: model evaluation and projections. J. Geophys. Res. Atmos. 118, 12458–12475.

Cai, W., Li, K., Liao, H., Wang, H., Wu, L., 2017. Weather conditions conducive to Beijing severe haze more frequent under climate change. Nat. Clim. Change 7 (4), 257–262.

Chang, C.P., Lu, M.M., 2012. Intraseasonal predictability of Siberian High and East Asian winter monsoon and its interdecadal variability. J. Clim. 25, 1773–1778.

Chen, H., Wang, H., 2015. Haze Days in North China and the associated atmospheric circulations based on daily visibility data from 1960 to 2012. J. Geophys. Res. Atmos. 120, 5895–5909.

Chernokulsky, A., Mokhov, I.I., Nikitina, N., 2013. Winter cloudiness variability over northern Eurasia related to the Siberian High during 1966-2010. Environ. Res. Lett. 8 045012.

Cheng, X., Zhao, T., Gong, S., Xu, X., Han, Y., Yin, Y., Tang, L., He, H., He, J., 2016. Implications of East Asian summer and winter monsoons for interannual aerosol variations over central-eastern China. Atmos. Environ. 129, 218–228.

Fiore, A.M., Jacob, D.J., Mathur, R., Martin, R.V., 2003. Application of empirical orthogonal functions to evaluate ozone simulations with regional and global models. J. Geophys. Res. Atmos. 108 (D14), 4431.

Gao, M., Carmichael, G.R., Saide, P.E., Lu, Z., Yu, M., Streets, D.G., Wang, Z., 2016. Response of winter fine particulate matter concentrations to emission and meteorology changes in north China. Atmos. Chem. Phys. 16 (18), 11837–11851.

Gao, H., Xiang, L., 2015. Influences of El Nino Southern Oscillation events on haze frequency in eastern China during boreal winters. Int. J. Climatol. 35 (9), 2682–2688.

Gong, D.Y., Ho, C.H., 2002. The Siberian High and climate change over middle to high latitude Asia. Theor. Appl. Climatol. 72 (1–2), 1–9.

Guo, J., Zhang, X., Wu, Y., 2011. Spatio-temporal variation trends of satellite-based aerosol optical depth in China during 1980-2008. Atmos. Environ. 45, 6802–6811.

Guo, J., Xia, F., Zhang, Y., Liu, H., Li, J., Lou, M., He, J., Yan, Y., Wang, F., Min, M., Zhai, P., 2017. Impact of diurnal variability and meteorological factors on the $PM_{2.5}$ - AOD relationship: implications for $PM_{2.5}$ remote sensing. Environ. Pollut. 221 (94), 94.

Hasanean, H.M., Almazroui, M., Jones, P.D., Alamoudi, A.A., 2013. Siberian high variability and its teleconnections with tropical circulations and surface air temperature over Saudi Arabia. Clim. Dynam. 41, 2003–2018.

Huang, K., Zhuang, G., Wang, Q., Fu, J., Lin, Y., Liu, T., Han, L., Deng, C., 2014. Extreme haze pollution in Beijing during January 2013: chemical characteristics, formation mechanism and role of fog processing. Atmos. Chem. Phys. Discuss. 14 (6), 479–486.

Jeong, J.H., Ou, T., Linderholm, H.W., Kim, B.M., Kim, S.-J., Kug, J.S., Chen, D., 2011. Recent recovery of the siberian high intensity. Journal of Geophysiccal Research-Atmosphere 116 D23102.

Jia, B., Wang, Y., Yao, Y., Xie, Y., 2015. A new indicator on the impact of large-scale circulation on wintertime particulate matter pollution over China. Atmos. Chem. Phys. 15, 11919–11929.

Kalnay, E., Kanamitsu, M., Kistler, R., Collins, W.D., Deaven, D.G., Gandin, L., Iredell, M., Saha, S., White, G., Woollen, J., Zhu, Y., Chelliah, M., Ebisuzaki, W., Higgins, W., Janowiak, J., Mo, K., Ropelewski, C., Wang, J., Leetmaa, A., Reynolds, R., Jenne, R., Joseph, D., 1996. The NCEP/NCAR 40-year reanalysis project. Bull. Am. Meteorol. Soc. 77, 437–471.

Kistler, R., Kalnay, E., Collins, W., Saha, S., White, G., Woollen, J., Chelliah, M., Ebisuzaki, W., Kanamitsu, M., Kousky, V., Dool, H., Jenne, R., Fiorino, M., 2001. The NCEP-NCAR 50-year reanalysis: monthly means CD- ROM and documentation. Bull. Am. Meteorol. Soc. 82, 247–267.

Lelieveld, J., Evans, J.S., Fnais, M., Giannadaki, D., Pozzer, A., 2015. The contribution of outdoor air pollution sources to premature mortality on a global scale. Nature 525, 367–371.

Li, R., Cui, L., Li, J., Zhao, A., Fu, B., Wu, Y., Zhang, L., Kong, L., Chen, J., 2017. Spatial and temporal variation of particulate matter and gaseous pollutants in China during 2014-2016. Atmos. Environ. 161, 235–246.

Li, J., Carlson, B.E., Lacis, A.A., 2015. How well do satellite AOD observations represent the spatial and temporal variability of $PM_{2.5}$, concentration for the United States? Atmos. Environ. 102, 260–273.

Ma, Z., Hu, X., Huang, L., Bi, J., Liu, Y., 2014. Estimating ground-level $PM_{2.5}$ in China using satellite remote sensing. Environ. Sci. Technol. 48 (13), 7436–7444.

Moss, R.H., Edmonds, J., Hibbard, K., Manning, M., Rose, S., Vuuren, D., Carter, T., Emori, S., Kainuma, M., Kram, T., Meehl, G., Mitchell, J., Nakicenovic, N., Riahi, K., Smith, S., Stouffer, R., Thomson, A., Weyant, J., Wilbanks, T., 2010. The next generation of scenarios for climate change research and assessment. Nature 463, 747–756.

Niu, F., Li, Z., Li, C., Lee, K., Wang, M., 2010. Increase of wintertime fog in China: potential impacts of weakening of the Eastern Asian monsoon circulation and increasing aerosol loading. J. Geophys. Res. 115 D00K20.

Nickolay, A. Krotkov, Mclinden, C., Li, C., Lamsal, L., Celarier, E., Marchenko, S., Swartz, W., Bucsela, E., Joiner, J., Duncan, B., Boersma, K., Veefkind, J., Levelt, P., Fioletov, V., Dickerson, R., He, H., Lu, Z., Streets, D., 2016. Aura OMI observations of regional SO2 and NO2 pollution changes from 2005 to 2015. Atmos. Chem. Phys. 16, 4605–4629.

Ronald, J., van der, A., Mijling, B., Ding, J., Koukouli, M., Liu, F., Li, Q., Mao, H., 2017. Cleaning up the air: effectiveness of air quality policy for SO2 and NOx emissions in China. Atmos. Chem. Phys. 17, 1775–1789.

Shen, L., Mickley, L.J., Tai, A.P.K., 2015. Influence of synoptic patterns on surface ozone variability over the eastern United States from 1980 to 2012. Atmos. Chem. Phys. 15, 13073–13108.

Shen, L., Mickley, L.J., Murray, L.T., 2017. Influence of 2000-2050 climate change on particulate matter in the United States: results from a new statistical model. Atmos. Chem. Phys. 17 (6), 1–26.

Tai, A.P.K., Mickley, L.J., Jacob, D.J., 2012. Impact of 2000-2050 climate change on fine particulate matter ($PM_{2.5}$) air quality inferred from a multi-model analysis of meteorological modes. Atmos. Chem. Phys. 12, 11329–11337.

Taylor, K.E., Stouer, R.J., Meehl, G.A., 2012. An overview of CMIP5 and the experiment design. Bull. Am. Meteorol. Soc. 93 (4), 485–498.

Wang, J., Christopher, S.A., 2003. Intercomparison between satellitederived aerosol optical thickness and $PM_{2.5}$ mass: implications for air quality studies. Geophys. Res. Lett. 30, 2095.

Wang, S., Zhao, B., Cai, S., Klimont, Z., Nielsen, C., Morikawa, T., Woo, J., Kim, Y., Fu, X., Xu, J., Hao, J., He, K., 2014b. Emission trends and mitigation options for air pollutants in East Asia. Atmos. Chem. Phys. 14 (13), 6571–6603.

Wang, Y.X., Zhang, Q., Jiang, J., Zhou, W., Wang, B., He, K., Duan, F., Zhang, Q., Philip, S., Xie, Y., 2014c. Enhanced sulfate formation during China's severe winter haze episode in January 2013 missing from current models. J. Geophys. Res. Atmos 119, 10425–10440.

Wang, L., Chen, W., 2014. An intensity index for the east Asian winter monsoon. J. Clim. 27 (6), 2361–2374.

Wang, L., Zhang, N., Liu, Z., Sun, Y., Ji, D., Wang, Y., 2014a. The influence of climate factors, meteorological conditions, and boundary-layer structure on severe haze pollution in the Beijing-Tianjin-Hebei region during January 2013. Advances in Meteorology 2014 (2014), 1–14.

Wang, H., Jiang, D., 2004. A new East Asian winter monsoon intensity index and atmospheric circulation comparison between strong and weak composite. Quat. Sci. 24 (1) 2004 (in Chinese).

Weaver, S.J., Nigam, S., 2008. Variability of the Great Plains low-level jet: large-scale circulation context and hydroclimate impacts. J. Clim. 21, 1532–1551.

Xie, Y.Y., Wang, Y., Zhang, K., Dong, W., Lv, B., Bai, Y., 2015. Daily estimation of ground-level PM2:5 concentrations over Beijing using 3 km resolution MODIS AOD. Environ. Sci. Technol. 49, 12280–12288.

Xu, X., Zhao, T., Liu, F., Gong, S., Kristovich, D., Lu, C., Guo, Y., Cheng, X., Wang, Y., Ding, G., 2016. Climate modulation of the Tibetan Plateau on haze in China. Atmos. Chem. Phys. 16, 1365–1375.

Xue, Y., Zhou, Z., Nie, T., Pan, T., Qi, J., Nie, L., Wang, Z., Li, Y., Li, X., Tian, H., 2016. Exploring the severe haze in beijing during December, 2015: pollution process and emissions variation. Environ. Sci. J. Integr. Environ. Res. 37 (5), 1593–1601 (in Chinese).

Yao, Y., Luo, Y., Huang, J., Zhao, Z., 2013. Comparison of monthly temperature extremes simulated by CMIP3 and CMIP5 models. J. Clim. 26 (19), 7692–7707.

Yin, Z., Wang, H., 2017. Role of atmospheric circulations in haze pollution in December 2016. Atmos. Chem. Phys. 17, 11673–11681.

Zou, Y., Wang, Y., Zhang, Y., Koo, J., 2017. Arctic sea ice, Eurasia snow, and extreme winter haze in China. Science Advances 3 (3), e1602751 2017.

Zhang, R.H., Qiang, L., Zhang, R.N., 2014. Meteorological conditions for the persistent severe fog and haze event over eastern China in January 2013. Sci. China Earth Sci. 57 (1), 26–35.